

n-alkanes on MgO(100). II. Chain length dependence of kinetic desorption parameters for small *n*-alkanes

Steven L. Tait

Department of Physics, University of Washington, Seattle, Washington 98195-1560

Zdenek Dohnálek

Chemical Sciences Division, Fundamental Sciences Directorate, Pacific Northwest National Laboratory, Richland, Washington 99352

Charles T. Campbell

Department of Chemistry, University of Washington, Seattle, Washington 98195-1700

Bruce D. Kay^{a)}

Chemical Sciences Division, Fundamental Sciences Directorate, Pacific Northwest National Laboratory, Richland, Washington 99352

(Received 25 October 2004; accepted 8 February 2005; published online 27 April 2005)

Coverage-dependent desorption-kinetics parameters are obtained from high-quality temperature-programmed desorption data for seven small *n*-alkane molecules on MgO(100). The molecules, C_NH_{2N+2} ($N=1-4, 6, 8, 10$), were each studied for a set of 29 initial coverages at a heating ramp rate of 0.6 K/s as well as at a set of nine ramp rates in the range of 0.3–10.0 K/s. The inversion analysis method with its least-squares preexponential factor (prefactor) optimization discussed in the accompanying article is applied to these data. This method allows for accurate determination of prefactors and coverage-dependent desorption energies. The prefactor for desorption increases dramatically with chain length from $10^{13.1}$ to $10^{19.1}$ s⁻¹ over the range of $N=1-10$. We show that this increase can be physically justified by considering the increase in rotational entropy available to the molecules in the gaslike transition state for desorption. The desorption energy increases with chain length as $E_d(N)=6.5+7.1N$, which implies an incremental increase of 7.1 ± 0.2 kJ/mol per CH₂. © 2005 American Institute of Physics.

[DOI: 10.1063/1.1883630]

INTRODUCTION

The interaction of small hydrocarbon molecules with surfaces is of interest for a wide range of applications including catalysis, atmospheric chemistry, geochemistry, and chemical sensing. Understanding the dependence of desorption energy on alkane chain length is a topic of current interest for these applications as well as for understanding the basic physics behind the chain length scaling. This chain length dependence has been explored by desorption of small alkane molecules from metal surfaces, such as Pt(111),^{1,2} Ru(001),³ Cu(100),^{4,5} and Au(111).⁶

Compared to work on metal surfaces, alkane adsorption on oxide surfaces has remained relatively unexplored. This in spite of the important role oxides play as support materials in catalytic applications. The exception is the work done by Slayton *et al.* to study the desorption of butane, hexane, and octane from aluminum oxide.⁷ There has also been an extensive study of *n*-alkane ($N=5-60$) desorption from the inert graphite surface by Paserba and Gellman.^{8,9}

In each of these previous studies a linear increase in the desorption energy with chain length is reported for the small *n*-alkanes ($N=1-12$). In these cases of nondissociative “phy-

sisorption” this increase can be interpreted as an additive van der Waals-type interaction between the alkane molecule and the substrate. As the chain length of the molecule increases, there are more methylene segments to interact with the substrate. This corresponds to the measured increase in the polarizability of these molecules with chain length, which is observed to be nearly linear in chain length.¹⁰ However, the *y*-intercept value of the desorption energy versus chain length (or polarizability) has been reported to be large. A comparison of these slopes and *y*-intercept values has recently been presented in the literature¹¹ and shows that these *y*-intercept values are often found to be several times greater than the incremental increase in energy per methylene segment. This has been noted in the literature, but a clear physical explanation for its origin has remained elusive.

One idea that has been discussed in the literature is that this *y*-intercept value is due to differences between methyl and methylene group adsorption (“end-group” effects).^{1,6,8,9} Lei *et al.*¹¹ have studied desorption of *n*-alkanes and cyclic alkanes ($c-C_NH_{2N}$) in the range of $N=3-12$ in order to address the issue of whether large *y*-intercept values could be due to end-group effects. They find that for desorption of both the linear and cyclic alkanes from the Pt(111) surface, the desorption energy increases linearly with *N*. They point out that the nonzero *y* intercept for the two cases is similar

^{a)} Author to whom correspondence should be addressed. Fax: (509)376-6066. Electronic mail: bruce.kay@pnl.gov

and conclude that the intercept cannot be attributed to differences in CH₃ versus CH₂ segment adsorption in the *n*-alkanes.¹¹

Fichthorn and Miron¹² have conducted detailed molecular-dynamics simulations of *n*-alkanes ($N=1-12$) from Au(111) and reported a sharp increase in preexponential factor (prefactor) with alkane chain length ($10^{12.2}$ for methane to $10^{16.0}$ for decane). They also demonstrate that if a prefactor of 10^{13} s^{-1} is assumed for analysis of temperature-programmed desorption (TPD) experiments (a common assumption traditionally), the calculated desorption energies come out to be artificially small and that this discrepancy increases with increasing chain length. The result is that the slope of the desorption energy versus chain length line is too small and the *y*-intercept value is large.

Here we present temperature-programmed desorption results for seven small *n*-alkane molecules ($N=1-4, 6, 8, 10$) on MgO(100). We will show that the common assumption of a prefactor of 10^{13} s^{-1} leads to a large nonzero energy intercept. Instead, we obtain the desorption prefactor for each molecule by simulating the TPD data from the results of our TPD analysis and varying the prefactor to optimize the fit of the simulation to the experimental data, as described in detail in the accompanying article.¹³ By allowing the prefactor to vary with chain length, a much more physically reasonable picture of desorption energy dependence on chain length (i.e., smaller *y* intercept) is obtained. The prefactor is found to increase by six orders of magnitude over the range of molecules studied. We show that such a significant prefactor increase with chain length can be understood by a simple statistical mechanical calculation of the rotational entropy increase for each molecule as it evolves from a translationally and rotationally hindered adsorbed state into a gas-phase molecule through a freely translating and freely rotating transition state.

EXPERIMENT

The experimental apparatus has been described in detail elsewhere.^{13,14} The TPD experiments in this work were conducted under ultrahigh-vacuum conditions, with base pressure $\sim 1 \times 10^{-10}$ Torr. Experimental procedures for growth of a high-quality MgO(100) film on a Mo(100) substrate as well as the sample temperature control and calibration are discussed in the accompanying article.¹⁴

The molecules studied are straight chain alkanes: methane, ethane, propane, *n*-butane, *n*-hexane, *n*-octane, and *n*-decane ($\text{C}_N\text{H}_{2N+2}$, $N=1-4, 6, 8, 10$). Liquid-phase molecules ($N=6, 8, 10$) were purified by several freeze-pump-thaw cycles. The beam nozzle was held at room temperature during deposition. The beam flux for each molecule is listed in Table I. During deposition, the sample was held at a temperature (listed in Table I) well below the multilayer desorption temperature (see Fig. 1) for that molecule. No dissociation of the molecules was observed on the MgO surface. Reflected flux of the molecular beam was measured by quadrupole mass spectrometer (QMS) in a line-of-sight position (*m/e* values and acquisition rates in Table I).

Temperature-programmed desorption experiments were

TABLE I. Experimental parameters for TPD experiments of *n*-alkanes on MgO(100). Shown for each of the seven molecules studied are values for the molecular-beam flux, F_{beam} ; the sample temperature during deposition, T_{dep} ; the mass spectrometer *m/e* measured during TPD; and the acquisition rate during TPD measurements, f_{aq} .

Alkane ($\text{C}_N\text{H}_{2N+2}$)	F_{beam} (ML/s)	T_{dep} (K)	<i>m/e</i>	f_{aq} (Hz)
Methane ($N=1$)	0.25	24	16	11
Ethane ($N=2$)	0.11	24	28	22
Propane ($N=3$)	0.21	24	29	22
Butane ($N=4$)	0.13	24	43	22
Hexane ($N=6$)	0.10	30	41	20
Octane ($N=8$)	0.18	115	43	20
Decane ($N=10$)	0.13	130	43	20

conducted by ramping the temperature of the sample at a rate of 0.6 K/s and measuring the desorption of the molecule by QMS in the same position and parameters as during deposition. For each molecule, TPD experiments were conducted at many initial coverages (29 unique coverages for each molecule) at a heating ramp rate of 0.6 K/s. In addition to these experiments at 0.6 K/s, we conducted TPD experiments at several other heating rates for each molecule. TPD were measured at eight heating ramp rates in the range of 0.3–10.0 K/s for six initial coverages for methane and seven initial coverages for ethane, propane, and butane. Three other heating rates (0.07, 0.3, and 1 K/s) were used at three initial coverages for hexane and decane, and at four initial coverages for octane. For each heating rate of 1.0 K/s or greater, it was necessary to make a small (≤ 4.5 K) correction to the thermocouple reading to accurately represent the average sample temperature, due to a temperature gradient on the sample. The procedure for empirically determining the magnitude of the needed correction is identical to that described in detail in the accompanying paper,¹³ except that here we determine the corrections from the leading edges of submonolayer desorption peaks rather than multilayer peaks. Briefly, the leading edges of a set of submonolayer desorption peaks for a given initial coverage at different heating ramp rates are aligned such that the curves fall on top of each other at their leading edge where the desorption rate had risen to about 10^{-3} ML/s (ML=monolayers), i.e., in the limit where the coverage on the surface is approximately equal to the initial coverage and so each of the experiments is at the same molecule coverage. This was possible because of the excellent dynamic range of the TPD data.¹³ This temperature correction was found to be approximately proportional to the heating rate and was also found to increase weakly with temperature. That is, the temperature gradient across the sample and hence the needed temperature correction were smallest for methane desorption measurements and increased with increasing alkane chain length (increasing desorption temperature, see Fig. 1). This is because the thermal conductivity of the metal substrate decreases and its heat capacity increases with increasing temperature.¹⁰

RESULTS

TPD spectra for desorption from MgO(100) are shown in Fig. 1 for (a) methane, (b) ethane, (c) propane, (d) butane,

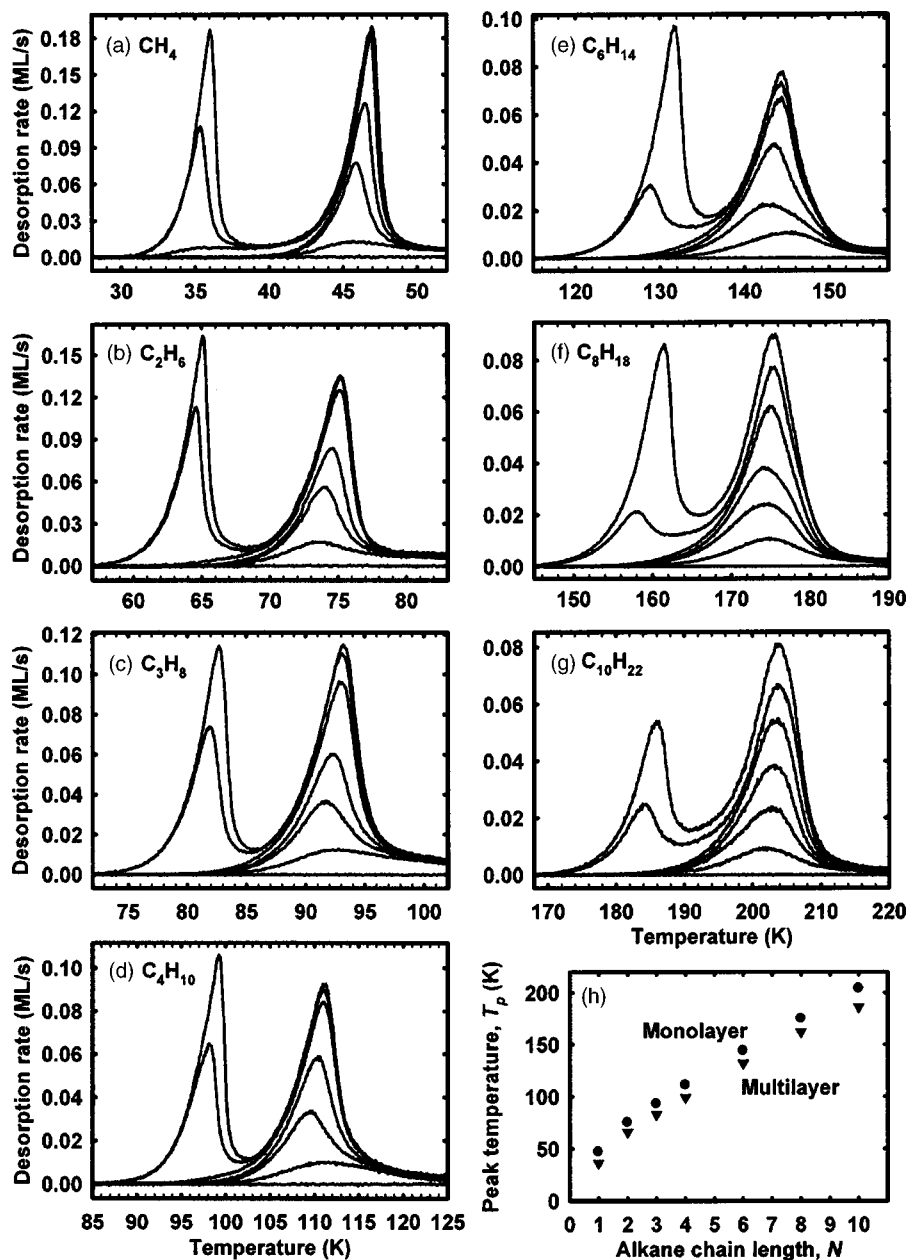


FIG. 1. TPD spectra of *n*-alkane molecules, C_NH_{2N+2} , on MgO(100) for $N =$ (a) 1, (b) 2, (c) 3, (d) 4, (e) 6, (f) 8, and (g) 10. Each panel displays TPD spectra recorded at 0.6 K/s for seven initial coverages. For clarity of presentation 22 other initial coverages are not shown. Panel (h) shows the desorption peak temperature of the two prominent desorption peaks (multilayer and monolayer) in each TPD set, plotted as a function of chain length, N .

(e) hexane, (f) octane, and (g) decane. For each molecule, seven representative spectra are plotted corresponding to seven initial coverages in the range of 0–2 ML. We recorded similar data at 22 other initial coverages for each molecule which are not shown here for clarity of presentation, but some of which were used in the following analysis. Note that the scales of both the temperature (horizontal) axis and the desorption rate (vertical) axis are different for each panel in Figs. 1(a)–1(g). In each set of TPD spectra in Figs. 1(a)–1(g), we see two distinct peaks corresponding to desorption of the multilayer of the molecule (low temperature) and desorption of its first monolayer (higher temperature). In Fig. 1(h), we have plotted the desorption peak temperature for the multilayer and monolayer peaks as a function of alkane chain length. Both of these increase monotonically with chain length. The ratio of the multilayer desorption peak temperature to the first-layer peak temperature is about 0.9 in each case. In the case of methane and propane for higher initial

coverages than those shown in Fig. 1, we are able to resolve the second-layer desorption peak from the multilayer desorption peak. In the cases of the other molecules, desorption from the second and higher layers was not resolved from the multilayer desorption peak. The shape of the multilayer peak is characteristic of zero-order (coverage-independent) desorption, where the leading edges of desorption peaks for several initial coverages align, then the desorption rate drops sharply when the multilayer is exhausted. However, the leading edges of the multilayer peaks for octane and decane are not aligned as well as those for the shorter chain molecules.

Observing the change in the TPD for the smallest alkanes ($N=1-4$) with increasing initial coverage, we see that the magnitude of the first-layer peak saturates before the multilayer peak begins to fill, i.e., the first-layer peak does not increase in height as the multilayer peak grows [see Figs. 1(a)–1(d), three largest initial coverages]. However, for the larger molecules studied ($N=6,8,10$) the first-layer peak

continues to grow even after the multilayer peak starts [see Figs. 1(e)–1(g)]. Also, the separation of the two peaks for the larger molecules is not as distinct as for the smaller molecules (desorption rate is nonzero between the peaks). This is due to the trapping of molecules in metastable structures on the surface with increasing coverage. It seems that the smaller molecules are able to migrate more easily on the surface than the larger molecules, and thus they are not kinetically prevented from moving into the most stable structure. The first-layer desorption peak line shape in most cases is characteristic of first-order desorption kinetics. The peak shape is self-similar and the peak position is constant for various initial coverages. Each first-layer peak shifts to higher temperature with increasing coverage due to attractive interactions between the adsorbate molecules. For several of the molecules, especially methane, ethane, propane, and butane, this is a noticeable shift causing the first-layer peak shape to appear to be more characteristic of zero-order desorption than first-order desorption.

We also note a high-temperature tail on the first-layer desorption peak for each of the molecules studied. It is clear from the coverage evolution of each molecule that this tail is *not* due to a limitation in pumping speed (>5000 L/s in this chamber), as the tail saturates in height at relatively low initial coverage and does not increase in size proportional to the first-layer peak. From the lowest initial coverage spectrum shown [most notably for methane, propane, and butane, Figs. 1(a), 1(c), and 1(d)], it is clear that this tail is a small, higher-temperature desorption peak, which we interpret to be due to desorption from defect sites on the surface. The relative size of this tail compared to the first-layer desorption peak decreases with increasing chain length, indicating that the adsorption of a smaller fraction of molecules is affected by the defect sites for the larger molecules. The saturation of this peak before the filling of the first-layer peak indicates that the molecules have sufficient mobility on the MgO(100) surface at low coverages to find the most energetically favorable adsorption site, although this may be less true for the larger molecules, as it is not clear that their tail completely saturates. The area of this “defect” peak is difficult to deconvolute from the first-layer peak, but is similar in fractional coverage to the density of defect sites on the MgO surface.¹³ It has been remarked previously that the amount of the adsorbate that is influenced by defect sites cannot be equated to the density of surface defects, as the binding of an adsorbate molecule in the vicinity of a defect-bound adsorbate molecule may also be influenced by the defect or several adsorbate molecules could be stabilized by one defect.¹⁴

To emphasize the importance of allowing the prefactor to vary with chain length, we have calculated desorption energies using the Redhead equation¹⁵ and assumed a constant prefactor of 10^{13} s⁻¹. These energies are plotted as triangles in Fig. 2(a) and increase linearly with chain length with a large *y*-intercept value. The dashed line is a linear fit to these data $E_d(N) = E_0 + \Delta EN$. Here the *y*-intercept value ($E_0 = 9.7$ kJ/mol) is more than twice as large as the incremental increase in chain length with each *C* segment ($\Delta E = 4.6$ kJ/mol·*C* segment). Large nonzero *y*-intercept values have been reported previously using this Redhead analysis,

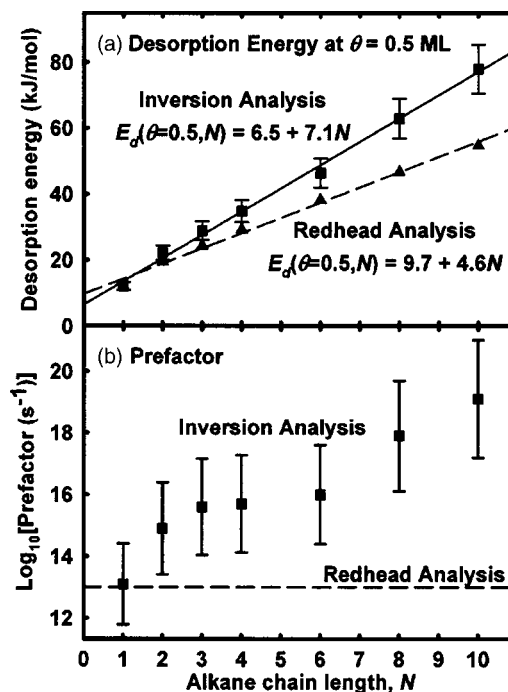


FIG. 2. Summary plots of (a) desorption energy and (b) prefactor vs chain length for desorption of small alkanes from MgO(100). The triangular symbols in (a) are desorption energies calculated from the Redhead equation and the monolayer peak temperatures and are fit by the dashed line. The square symbols in (a) represent the desorption energy from our inversion-optimization analysis evaluated at 0.5-ML coverage and are fit by the linear function represented as a solid line. The error bars correspond to the $\pm 10\%$ sensitivity in $\log(\text{prefactor})$ from this analysis. In (b) we have plotted the prefactors used in the inversion analysis to get the best match to experiment. These are shown as square symbols with error bars representing the $\pm 10\%$ sensitivity of these numbers. The dashed line is drawn to illustrate the common TPD analysis assumption of a prefactor of 10^{13} s⁻¹.

but no clear physical justification for a large nonzero intercept has been offered. We will demonstrate that this intercept value can be substantially smaller when the prefactor is allowed to vary with chain length in the experimental data analysis.

Calculation of the coverage-dependent desorption energy was made for each molecule by the inversion-optimization analysis procedure described in the accompanying article.¹³ Briefly, a TPD spectrum for an initial coverage greater than one ML was used to calculate desorption energy as a function of coverage by inverting the Polanyi–Wigner equation and assuming some (coverage-independent) preexponential factor. Then the resulting energy versus coverage less than one monolayer (ML) and the χ^2 error, defined as the sum of the squares of the differences between simulation and experimental data points, is calculated. This is repeated for several assumed values of prefactor until a well-defined minimum in χ^2 is found, giving the “best-fit” prefactor. That is, the prefactor is treated as a variational parameter to minimize the residual error between the experimental and simulated TPD data.

The log of the best-fit prefactor for each molecule is plotted as a function of alkane chain length in Fig. 2(b). The error bars correspond to $\pm 10\%$ of the log of the prefactor, which we consider to be an upper limit on the uncertainty in

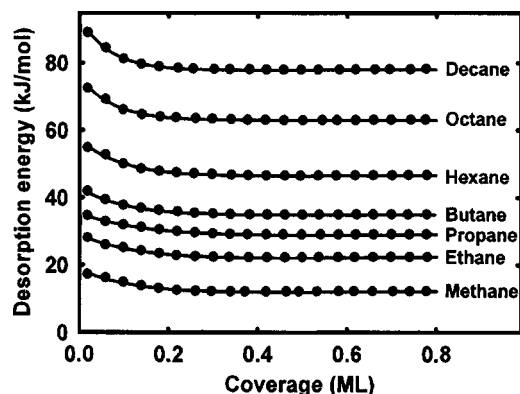


FIG. 3. Desorption energy vs adsorbate coverage for seven alkane molecules studied on MgO(100). Desorption energies were calculated using the inversion method for every data point in the TPD data using the best-fit prefactor shown in Fig. 2(b). For clarity of presentation, desorption energies at only 20 coverages in the interval of 0–0.8 ML are shown as solid points. The solid lines are fits to twice as many coverage points in that interval. The fit function is given in the text as Eq. (1) and the parameters of the fits are listed in Table II.

the prefactor due to experimental error.¹³ We see that the prefactor increases by six orders of magnitude over the range of molecules studied here. The dramatic increase of prefactor with chain length highlights the importance of allowing the value of the prefactor to vary with chain length in the TPD analysis. Much of the previous work to study TPD of the small alkanes has assumed a constant prefactor value of 10^{13} s^{-1} [indicated by a dashed line in Fig. 2(b)].

Using this best-fit prefactor, we calculate the desorption energy versus coverage for each of the molecules studied, which we have plotted in Fig. 3 (circular points) over the coverage range of 0–0.8 ML. The solid lines represent fits to an empirical equation as described further below. We note that the general line shape of this energy curve is similar for each molecule although the energy increases monotonically with alkane chain length. In each case the energy decreases steeply with increasing coverage in the range of approximately 0–0.2 ML. This corresponds to the coverage range where molecules are desorbing from defect sites on the surface as well as from the MgO terrace sites. The energy in this range represents a convolution of the desorption energy on the terrace and the desorption energies of the various species of defect sites. Above 0.3 ML the desorption energy is nearly constant with coverage as the molecules are desorbing from the MgO(100) terrace sites. However, there is a very small positive slope ($<1\%$) in each curve, due to attractive interactions between the adsorbate molecules. We summarize the desorption energy at 0.5-ML coverage for each molecule versus chain length in Fig. 2(a) (square symbols). The solid line in Fig. 2(a) is a linear fit to the desorption energies. The desorption energy increases nearly linearly with alkane chain length. The slope of this line is $7.1 \pm 0.2 \text{ kJ/mol} \cdot C$ segment and it has a *y*-intercept value of $6.5 \pm 1.1 \text{ kJ/mol}$. It is also instructive to consider this energy increase as a function of the polarizability of the alkanes, as plotted in Fig. 4. Again the dependence is linear, with a *y*-intercept value comparable to the slope.

The simulated spectra from the best-fit prefactors and

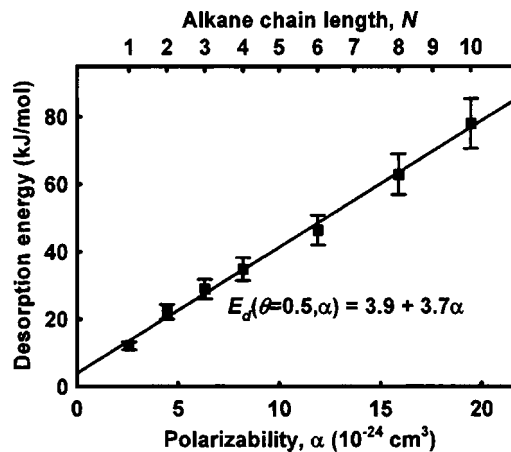


FIG. 4. Summary plot of desorption energy vs polarizability for small alkane desorption from MgO(100). The square symbols represent the desorption energy from our inversion-optimization analysis evaluated at 0.5-ML coverage, as in Fig. 2(a), and are fit by the linear function represented as a solid line. The error bars correspond to the $\pm 10\%$ sensitivity in $\log(\text{prefactor})$ from this analysis. Polarizabilities obtained from Ref. 10.

coverage-dependent energies (Fig. 3) are plotted for each alkane as solid lines in Figs. 5(a)–5(g) along with the experimental data as solid points. We see that for the best-fit prefactor values, agreement between simulation and experiment is very good, demonstrating the reliability of our inversion-optimization analysis method over this range of alkane chain lengths. The line shapes of the desorption peaks in each case are reproduced very well by the simulation. The coverage dependence of the desorption-kinetics parameters is essential for capturing the subtle deviations in the peak shape from ideal TPD line shapes.

In addition to varying the initial coverage in the TPD experiments, we also conducted experiments at various heating ramp rates (eight rates in the range of 0.3–10.0 K/s). We have plotted representative TPD data from these experiments as points in Figs. 6(a)–6(g). We have used the results of the inversion analysis to simulate corresponding TPD spectra. These simulations, which are plotted as solid lines in Fig. 6, were made using the desorption energy versus coverage curves discussed above (Fig. 3) which were calculated by inversion of TPD data taken at 0.6 K/s. We see that the agreement between simulation and experiment is excellent for each molecule, demonstrating the robustness of the inversion-optimization analysis result over a wide range of heating ramp rates and chain length. The desorption peak shape is reproduced well by the simulation, even at high ramp rates. The high-temperature tail due to desorption from defect states is matched well by the simulation and scales appropriately with heating rate.

We further analyzed the coverage dependence of E_d . Each energy curve can be fitted to the analytic form

$$E_d(\theta) = E_0 + \gamma\theta + E_{\text{def}}e^{-\theta/\theta_{\text{def}}}. \quad (1)$$

The fit functions are shown as solid lines in Fig. 3 and the fitting parameters are listed in Table II. For each molecule this function fits the desorption energy very well ($\chi^2 > 0.99$). The first term E_0 represents the desorption energy one would obtain by extrapolating the linear region of the

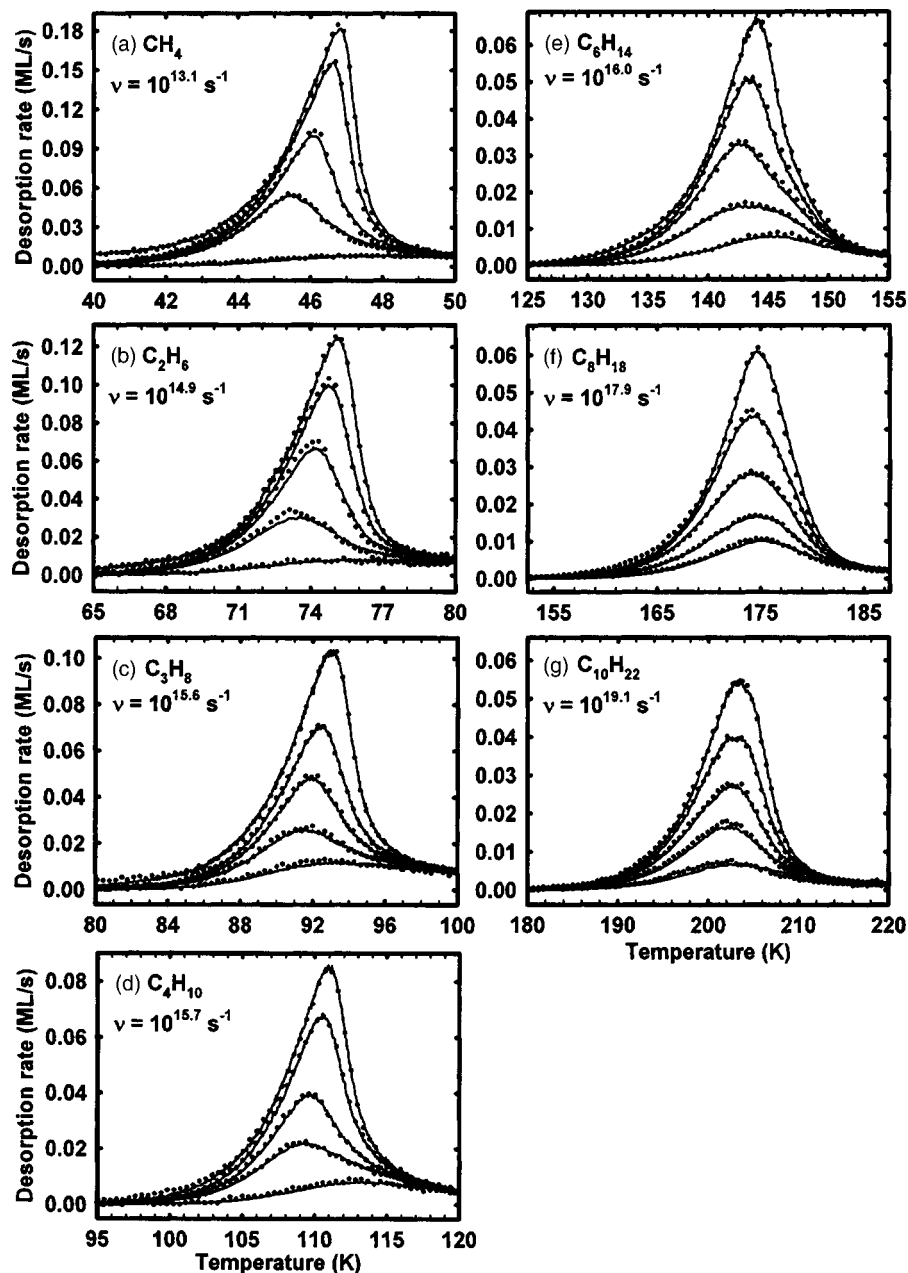


FIG. 5. TPD spectra of *n*-alkane molecules on MgO(100) at five initial coverages each ($\theta_0 \approx 0.2, 0.4, 0.6, 0.8, 1.0$ ML) at heating rate of 0.6 K/s. The points are experimental data and the solid lines are TPD simulations based on the prefactor and calculated coverage-dependent desorption energy obtained from the inversion-optimization method discussed in the text.

coverage-dependent energy curve back to the limit of zero coverage. This is the number that could most readily be interpreted as the activation energy for desorption of an isolated adsorbate from a MgO(100) terrace site (i.e., in the absence of defect sites and adsorbate-adsorbate interactions). In Fig. 7, E_0 is plotted as a function of alkane chain length. We see that this parameter increases linearly with alkane chain length (N) due to the increasing number of CH_2 -MgO interactions. It can be fitted well by the function $E_0 = 5.4 + 7.2N$ (shown as solid line in Fig. 7). The factor γ in the second term of Eq. (1) is the increase in desorption energy per ML increase in coverage due to lateral interactions between adsorbates. Its positive sign indicates an attractive interaction between alkane molecules on the MgO(100) surface. This number decreases with chain length, but not smoothly. This should not be interpreted as a decrease in intermolecular attraction at fixed separation with increasing molecule size, since the density of molecules in the mono-

layer decreases with increasing chain length and the intermolecular spacing is not necessarily constant with increasing chain length.

The factor E_{def} in the third term of Eq. (1) is the energy difference between E_0 and the measured desorption energy at zero coverage, $E_d(0)$, and is related to the difference between the adsorption energy of an alkane molecule adsorbed on a MgO terrace site compared to one adsorbed at a defect site. This value remains relatively constant for $N=1-3$ (see Table II), but then increases linearly with chain length by a factor of two in the range of $N=3-10$. It may be more instructive to consider the behavior of the ratio $(E_0 + E_{\text{def}})/E_0$, which compares the adsorption energy of a molecule at a defect site ($E_0 + E_{\text{def}}$) to that of a molecule at a terrace site (E_0). This ratio (also shown in Table II) decreases from 1.7 to 1.2 from $N=1-3$, but has a constant value of 1.2 in the range of $N=3-10$. The factor θ_{def} corresponds to the rate at which the influence of defect sites on the energy decays with increasing

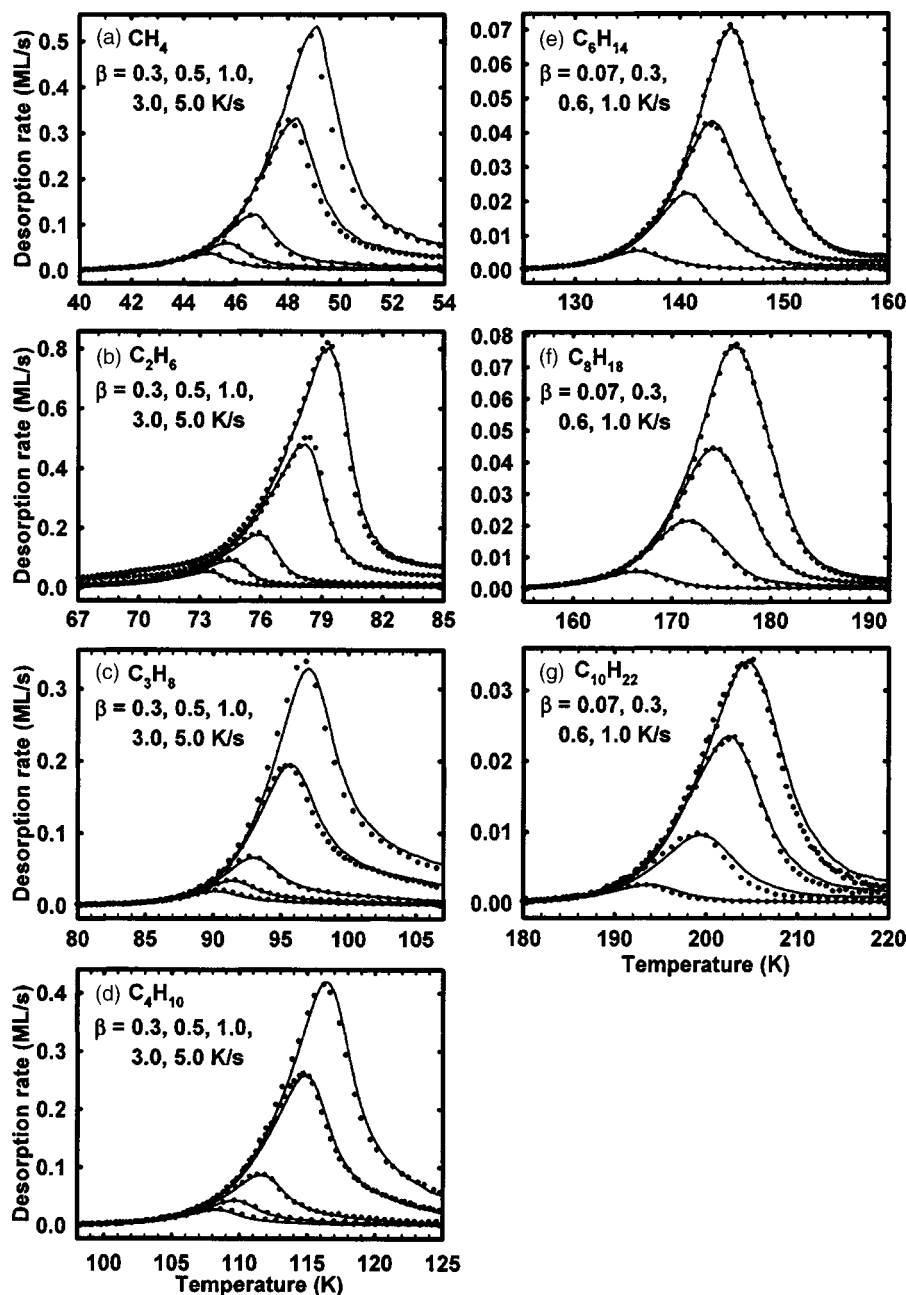


FIG. 6. TPD spectra of *n*-alkane molecules on MgO(100) recorded at several heating ramp rates: 0.3, 0.5, 1.0, 3.0, and 5.0 K/s in (a)–(d) and 0.07, 0.3, 0.6, and 1.0 for (e)–(g). For each of the spectra shown for a given molecule the initial coverages were (a) 0.52, (b) 0.90, (c) 0.60, (d) 0.73, (e) 0.71, (f) 0.80, and (g) 0.50 ML. The points are experimental data and the solid lines are TPD simulations based on the prefactor and calculated coverage-dependent desorption energy obtained from the inversion-optimization method discussed in the text.

coverage. It is related to the density (fractional area) of defect sites on the oxide surface as well as to the degree to which defect sites influence the adsorption of molecules that are near molecules adsorbed at defects. This number decreases with chain length (see Table II) probably because a single molecule of longer chain length can occupy more defect sites than the smaller molecules or because a single defect site can influence a larger number of the smaller alkanes compared to the longer alkanes.

A common technique for determining a prefactor and desorption energy is to make TPD measurements at many different heating rates and use the Redhead equation to extract the prefactor and desorption energy from the dependence of the desorption peak temperature on heating rate.^{15–17} This method has been used in several previous studies of the desorption of *n*-alkanes, C_NH_{2N+2} .^{3,7,8,11} The Polanyi–Wigner equation is evaluated at the desorption peak temperature, T_p , and rearranged in an Arrhenius form

$$\ln\left(\frac{\beta}{T_p^2}\right) = -\ln\left(\frac{E_d}{k_B\nu}\right) - \frac{E_d}{k_B T_p}, \quad (2)$$

where β is the heating rate and k_B is the Boltzmann constant. Implicit in this analysis is the assumption of coverage-independent desorption-kinetics parameters (ν and E_d). We have compiled the peak temperatures T_p for the TPD data shown in Fig. 6 and found that the points of $\ln(\beta/T_p^2)$ vs $1/T_p$ (not shown) fit well to a line. The slope and y intercept of this line yield the desorption energies and prefactors plotted as open diamonds in Figs. 8(a) and 8(b), respectively. The results from the inversion analysis are plotted in Figs. 8(a) and 8(b) as solid squares with error bars. We see that the results of the variable ramp rate method are in agreement with the results of the inversion analysis within the errors of the two analysis methods.

Coverage-dependent values for both prefactor and desorption energy can be obtained from another common

TABLE II. Parameter values for best fit of analytic function given in Eq. (1) to the experimentally obtained coverage-dependent desorption energies for each alkane studied.

Alkane (C _N H _{2N+2})	E_0 (kJ/mol)	γ (kJ/mol·ML)	E_{def} (kJ/mol)	θ_{def} (ML)	$(E_0 + E_{\text{def}})/E_0$
Methane ($N=1$)	11.1	1.53	7.53	0.124	1.68
Ethane ($N=2$)	21.3	1.46	7.72	0.126	1.36
Propane ($N=3$)	28.0	1.40	7.34	0.146	1.26
Butane ($N=4$)	34.5	0.566	8.37	0.101	1.24
Hexane ($N=6$)	46.0	0.843	11.1	0.0972	1.24
Octane ($N=8$)	62.9	0.206	12.9	0.0745	1.21
Decane ($N=10$)	77.6	0.587	15.7	0.0679	1.20

method referred to as complete analysis.^{18,19} This technique consists of measuring TPD over a wide range of coverages and/or heating ramp rates to allow measurement of $d\theta/dt(T, \theta)$ for various combinations of θ and T from which the desorption energy and prefactor can be calculated for discrete coverages.²⁰ A significant disadvantage to this complete analysis approach is that kinetic parameters are obtained only at discrete coverage values, which makes it difficult to accurately describe the desorption kinetics if these parameters vary rapidly in coverage, as in the present case. The inversion analysis that we have described here calculates a desorption energy value for each point on the TPD spectrum. We have carried out the complete analysis on our data and at high coverages ($\theta > 0.4$) obtained results that are generally in good agreement with the inversion analysis result. As discussed previously, at low coverages the complete analysis does not work well.¹³ The inversion method presented above produces reliable coverage-dependent desorption energy results at continuous coverages over the full submonolayer coverage range.

DISCUSSION OF PREFACTOR DEPENDENCE ON CHAIN LENGTH

We present here a physical explanation for the dramatic prefactor increase observed with increasing alkane chain length. The preexponential factor for a desorption process can be calculated from elementary transition state theory as²¹

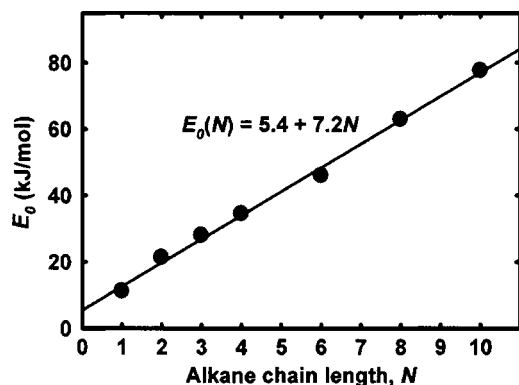


FIG. 7. Desorption energy fit parameter E_0 plotted as a function of alkane chain length, N . E_0 is the y -intercept value for the fit of Eq. (1) to the $E(\theta)$ result for each of the molecules studied (see Fig. 3). The solid line is a linear fit to these points.

$$\nu_{\text{TST}} = \left(\frac{k_B T}{h} \right) \frac{q^\ddagger}{q_{\text{ads}}}, \quad (3)$$

where q_{ads} and q^\ddagger are single-particle partition functions for the adsorbed (initial) state and the transition state, respectively, calculated at temperature T . Note that the degree of freedom along the reaction coordinate (normal to surface) is omitted from the calculation of q^\ddagger . In the case of a desorption process with no activation free-energy barrier to adsorption, as in the present case, the transition state is equivalent to the final state of the molecule, namely, its gas phase, without this one translational degree of freedom. In common TPD experiments of small molecules (CO, N₂, and H₂), the ratio of the partition functions is commonly assumed to be nearly unity (i.e., entropy is nearly the same in gas and adsorbed states), in which case the above expression gives a prefactor of about 10^{13} s⁻¹ for room-temperature desorption. However, when it has actually been measured carefully, it often has

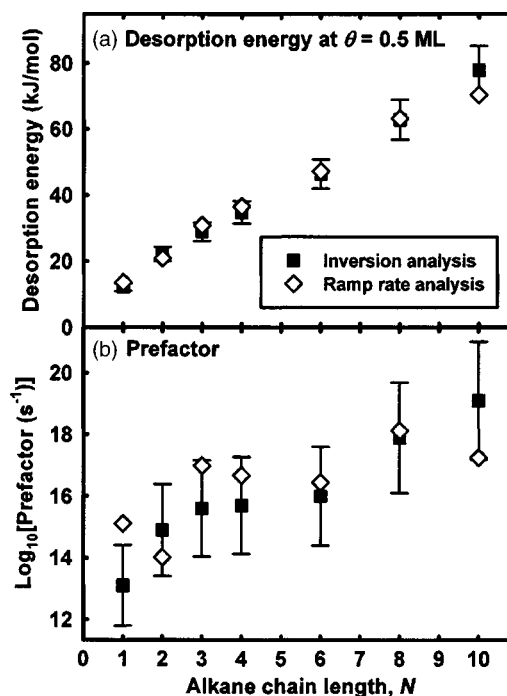


FIG. 8. Summary plots of (a) desorption energy and (b) prefactor vs chain length to compare results from inversion-optimization analysis (solid squares) and Redhead heating ramp rate analysis (hollow diamonds). The error bars for the ramp rate analysis are not shown but are estimated to be comparable in magnitude to the error bars of the inversion analysis.

TABLE III. Symmetry numbers, σ ; principle moments of inertia, I_x , I_y , and I_z ; monolayer peak desorption temperatures, T_p ; rotational partition functions, q_{rot} ; and translational partition functions, q_{trans} , for small *n*-alkanes ($N=1-10$).

Alkane ($\text{C}_N\text{H}_{2N+2}$)	σ	I_x (amu \AA^2)	I_y (amu \AA^2)	I_z (amu \AA^2)	$q_{\text{rot}}(300 \text{ K})$	T_p (K)	$q_{\text{rot}}(T_p)$	$q_{\text{trans}}(T_p)$
Methane ($N=1$)	12	3.17	3.17	3.17	37.2	47	2.30	39.7
Ethane ($N=2$)	6	6.46	25.3	25.3	844	75	105	148
Propane ($N=3$)	2	17.7	58.4	66.6	10 400	93	1790	337
Butane ($N=4$)	2	25.1	133	145	27 400	111	6170	626
Pentane ($N=5$)	2	30.5	253	268	56 700	128 ^a	15 800 ^a	975 ^a
Hexane ($N=6$)	2	37.4	430	449	106 000	144	35 200	1470
Heptane ($N=7$)	2	43.1	675	697	178 000	160 ^a	69 200 ^a	2020 ^a
Octane ($N=8$)	2	49.8	1000	1020	282 000	175	125 000	2740
Nonane ($N=9$)	2	55.5	1410	1440	420 000	190 ^a	212 000 ^a	3590 ^a
Decane ($N=10$)	2	62.1	1930	1960	605 000	204	339 000	4490

^aTPD experiments were not conducted for $N=5, 7$, and 9 . In these cases, T_p is obtained by quadratic interpolation of T_p values for other alkanes.

been found to be more than two orders of magnitude larger,²² suggesting that the ratio of partition functions is large. Recent molecular dynamics and transition state theory calculations by Fichthorn and Miron predict a significant increase in prefactor with chain length, consistent with Fig. 8, which they attribute to increasing differences between the adsorbate and transition state entropies.¹² This occurs because the adsorbed molecules are relatively hindered in translational and/or rotational degrees of freedom compared to the gas phase. Upon desorption, the vibrational modes associated with the hindered translations and rotations in the adsorbed state will be converted to free translational and rotational modes in the gas phase. These free motions will contribute much more to the partition function than the vibrations in the adsorbed state and the ratio $q^\ddagger/q_{\text{ads}}$ can be very large. Interpreting the strong prefactor increase in Fig. 2(b) using Eq. (3) implies that the ratio of these partition functions can increase by more than a factor of 10^5 over the range of methane to decane. Below, we interpret this in terms of the degrees of motional freedom in the initial adsorbed state using statistical thermodynamics.

Calculation of partition functions

We begin by considering various contributions to the molecular partition function. At the temperatures in question for these desorption processes ($<230 \text{ K}$), there is insufficient thermal energy to excite with large probability the intramolecular vibrational or electronic modes in the molecules either in the gas phase or the adsorbed phase. Therefore these partition functions can be taken to be unity in both states.

The translational partition function for a molecule in a container is²³

$$q_{\text{translational}}^{3\text{D}} = \left(\frac{2\pi mk_B T}{h^2} \right)^{3/2} V = \frac{V}{\Lambda^3}, \quad (4)$$

where m is the mass of the molecule, V is the volume of its container, and Λ is the thermal wavelength of the molecule. In two dimensions the translational partition function is²³

$$q_{\text{translational}}^{2\text{D}} = \frac{A}{\Lambda^2}, \quad (5)$$

where the molecule is confined to an area A . In this case, we can calculate a molecular partition function by assuming that the molecules behave on the surface as an ideal gas and taking A to be the area occupied by one mole of molecules on the surface at 1.0-ML coverage. This area can be estimated from the bulk packing density of each molecule (ignoring perturbation to the bulk packing due to the MgO lattice). This is equivalent to calculating the molar translational partition function using the standard state (i.e., the reference state defining unity activity) $\theta=1 \text{ ML}$, which is the appropriate choice since the concentration term in the rate is $k\theta$ (first-order desorption kinetics).²⁴ In this way the translational partition function of a two-dimensional gas of each *n*-alkane in the range of $N=1-10$ is calculated at the corresponding desorption temperature (see Table III). We see that the translational partition function increases by only two orders of magnitude over the range of chain lengths studied here. Hence, the translational contribution to the molecular partition function alone cannot account for the large increase in prefactor we observe over this range of chain lengths.

As shown below, the rotational partition function has a much stronger chain length dependence. Under the rigid-rotor assumption we calculate the rotational partition functions for the alkane molecules. Assumption of rigid molecule conformation simplifies calculation of the molecules' moments of inertia and hence their prefactors, but ignores effects of conformational entropy which will be discussed below. We choose Cartesian axes which pass through the molecule's center of mass and diagonalize the moment of inertia matrix (products of inertia are zero) to obtain the principle moments of inertia for the three axes, I_A , I_B , and I_C . Alternatively, one could consider this as orienting the coordinate space so that the moments of inertia about each of the three axes are the principal moments of the molecules. We take this approach to simplify notation. The approximate orientation of the axes is illustrated by the ball and stick cartoon of hexane in Fig. 9. The C atom plane is defined to be the x - y

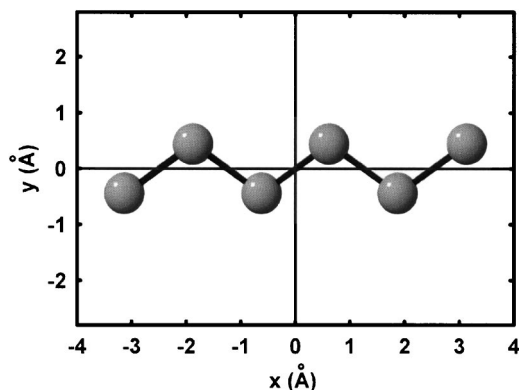


FIG. 9. Ball and stick model of *n*-hexane (C_6H_{14}). The coordinate system is defined such that the origin lies at the center of mass of the molecule and the C atoms (gray spheres), which are coplanar, lie in the x - y plane. The x axis is defined to be parallel to the axis of the molecule. The positive z axis is oriented out of the page. Hydrogen atoms are not shown for clarity of presentation.

plane with the x axis parallel to the molecule axis. The z axis is oriented out of the page in Fig. 9. The moment of inertia for rotation about the x axis is given by

$$I_x = \sum_i m_i (y_i^2 + z_i^2), \quad (6)$$

where the summation is taken over all of the atoms in the molecule. Analogous equations are constructed for moments of inertia about the y and z axes. The calculated moments are listed in Table III and displayed versus chain length as a log-log plot in Fig. 10. To calculate these moments, we have used published values for the alkane bond angles (109.5°) and bond lengths (C–C: 1.541 \AA ; C–H: 1.091 \AA in CH_4 , 1.101 \AA in $-CH_3$ units, and 1.073 \AA in $-CH_2-$ units).¹⁰

The x axis is in the C atom plane and runs along the axis of the molecule. The corresponding principle moment of inertia has a relatively weak chain length dependence, increasing only by a factor of 20 over the range of molecules studied. For the larger molecules ($N \geq 3$) this moment increases approximately linearly. As the size of the alkane chain increases, the distance of the added CH_2 groups from the x axis

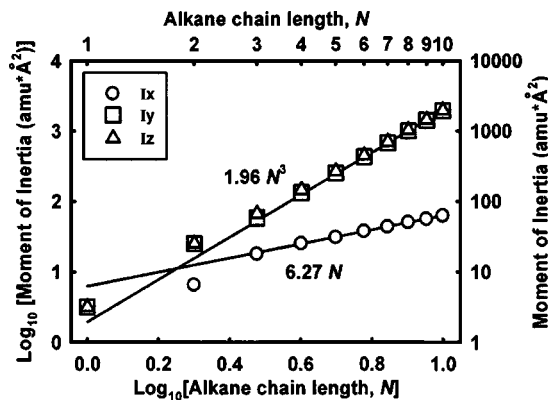


FIG. 10. Log-log plot of the moments of inertia for rigid small alkane molecules ($N=1-10$). The three symbols represent principle moments of inertia about the x (circles), y (squares), and z (triangles) axes. The axes are defined in the text and are illustrated in Fig. 9. The lines are a third-degree power-law fit to the I_y and I_z points for $N=3-10$ and a first-degree power-law fit to the I_x points in the same chain length range.

does not increase. Hence in the summation in Eq. (6), mass is increasing as the chain length increases, but the distance term is nearly constant for each CH_2 group. In Fig. 10, we have fitted the I_x values for chain lengths $N \geq 3$ to a first-degree power-law form ($y=ax$), shown as a solid line, to illustrate the linear dependence of I_x in this range. Rotation about the x axis can be thought of as a “log roll” mode in which most of the mass of the molecule is very near the rotational axis. However, in order for the log roll motion to occur on the surface for propane and the longer molecules, about half of the atoms in the molecule would have to move a significant distance away from the substrate, which would correspond to a significant potential energy cost. Thus the log roll or x -axis rotation is unlikely for propane and the larger molecules.

The y axis is perpendicular to the long axis of the molecule and also lies in the plane of C atoms. Rotation about the y axis would be a “cartwheel” or end-over-end rotation. Since both the mass and the distance of new chain segments from the center of mass increase linearly with N , the moment of inertia about the y axis scales as N^3 . A third-degree power-law fit ($y=ax^3$) to the I_y and I_z (see below) values in the range of $N \geq 3$ is shown as a solid line in Fig. 10 and shows very good agreement to these points. This cartwheel motion in the adsorbed state is very unlikely for any of the alkanes except methane, since all of the molecules except for one CH_3 group would have to move a significant distance from the surface. There would be a large energy cost in making such a motion.

The z axis is perpendicular to the C atom (x - y) plane. The moment of inertia about this axis also scales like N^3 for the larger molecules, analogous to the scaling of I_y . This “helicopter” rotational mode will be much more accessible in the adsorbed state since the molecule will maintain a nearly constant distance from the substrate, but corrugation of the surface potential will hinder this mode.

To simplify calculation of these moments of inertia, we have assumed that the molecule moves as a rigid rotor. This assumption will be valid for most of these molecules at the temperatures studied, but for the larger molecules, which desorb at higher temperatures, there will be some conformational changes in the structure of the molecule due to rotations about the interior C–C bonds (*trans-gauche* conformers). From bond rotation dynamic parameters for butane, which have been well studied,²⁵ we estimate that the most probable conformation for the smaller molecules will be the straight (all-*trans*) configuration, whereas for octane and decane the most probable configuration is to have at least one *cis* configuration. Such configurations will slightly reduce the moments of inertia of the molecule and thereby reduce the rotational partition function slightly. We have also estimated the contribution of C–C bond rotations to the molecular partition function (configurational entropy) and have found that this will contribute a factor of less than 5.6 for decane (compared to one for methane). The effects of C–C bond rotation to reduce the moments of inertia and contribute to the partition function are both minimal and so the assumption of rigid molecules in our calculation of the rotational partition function is well justified. A detailed description of

TABLE IV. Summary of experimentally obtained desorption energies (at $\theta=0.5$ ML) and prefactors for each of the alkanes studied. Also shown are values for the prefactor calculated for $N=1-10$ under various model assumptions described in the text.

Alkane (C_NH_{2N+2})	Experiment		Prefactor models			
	E_d (kJ/mol)	ν_{opt} (s^{-1})	$k_B T/h$ (s^{-1})	ν_{min} (s^{-1})	ν_{rotor} (s^{-1})	ν_{max} (s^{-1})
Methane ($N=1$)	12.1	13.1	12.0	12.0	12.4	14.0
Ethane ($N=2$)	22.2	14.9	12.2	13.1	14.2	16.4
Propane ($N=3$)	29.0	15.6	12.3	14.3	15.5	18.1
Butane ($N=4$)	34.9	15.7	12.4	14.7	16.2	19.0
Pentane ($N=5$)	40.8 ^a	15.9 ^a	12.4 ^a	15.0 ^a	16.6 ^a	19.6 ^a
Hexane ($N=6$)	46.4	16.0	12.5	15.3	17.0	20.2
Heptane ($N=7$)	54.6 ^a	17.0 ^a	12.5 ^a	15.5 ^a	17.4 ^a	20.7 ^a
Octane ($N=8$)	62.9	17.9	12.6	15.7	17.7	21.1
Nonane ($N=9$)	70.4 ^a	18.5 ^a	12.6 ^a	15.9 ^a	17.9 ^a	21.5 ^a
Decane ($N=10$)	77.9	19.1	12.6	16.0	18.2	21.8

^aTPD experiments were not conducted for $N=5, 7$, and 9 . In these cases, ν_{opt} obtained by linear interpolation of surrounding values, E_d calculated from Eq. (2), and prefactor models calculated using interpolated desorption temperatures listed in Table III.

the statistical mechanics of flexible chain molecules²⁶ is beyond the scope of this paper.

The rotational partition function of a three-dimensional rigid rotor^{21,23,24} is expressed as

$$q_{\text{rotational}} = \frac{\pi^{1/2}}{\sigma h^3} (8\pi^2 k_B T)^{3/2} (I_x I_y I_z)^{1/2} \\ = \frac{\pi^{1/2}}{\sigma} \left(\frac{T}{\Theta_x} \frac{T}{\Theta_y} \frac{T}{\Theta_z} \right)^{1/2}. \quad (7)$$

The symmetry factor, σ , can be thought of classically as the number of indistinguishable rotational configurations for the molecule, and so it prevents overcounting. For methane, the symmetry number is 12 because there are three indistinguishable rotational configurations about each C–H bond. Other symmetry numbers are given in Table III. The rotational partition functions for each of the molecules studied have been calculated at room temperature for comparison (see Table III). We see that this partition function increases by more than four orders of magnitude in the range studied due to the increase in the moment of inertia. If the partition functions are calculated at the desorption temperatures of the molecules this effect is more pronounced: the rotational partition function for decane is greater than that for methane by more than a factor of 10^5 (Table III).

Models for calculation of prefactor

In order to simplify calculation of the partition functions for this process we assume that in the transition state (gas phase) the molecules behave as a freely rotating three-dimensional (3D) gas (translational dimension along the reaction coordinate neglected in calculating transition state partition function). In order to accurately calculate the partition functions of the molecules in the adsorbed state a detailed knowledge of the interaction potential would be required.^{12,27} Such a study is beyond the scope of the present work. Nonetheless we can make certain assumptions about the degrees of freedom of the molecules in the adsorbed

(initial) state which will allow us to determine upper and lower limits for the possible range of prefactors. We will show that these limits bound the experimental results presented above.

As discussed above, the molecules are considered to be 3D rigid rotors in the gas phase; that is, they have three translational plus three rotational degrees of freedom. Upon adsorption at low temperature, all six degrees of freedom become vibrational modes, the so-called hindered translations and hindered rotations. At the desorption temperatures, however, the corresponding energy barriers may be small compared to $k_B T$, so that these motions may be effectively “free.” Clearly, this depends on the corrugation of the interaction potential, a detailed knowledge of which would be required to determine the true nature of the adsorbate motion. One of the translational degrees of freedom in the transition state is the reaction coordinate and is not considered in calculating the translational partition function for the transition state, as discussed above. That degree of freedom will correspond to a vibrational mode in the adsorbed state which we neglect by taking its partition function to be unity in each of the models discussed below. Thus, in either the adsorbed or transition state, the molecule is considered to have at most two translational and three rotational degrees of freedom.

The most straightforward picture is to consider the adsorbate molecules as being completely immobile on the surface. In this case the molecules are not free to translate or rotate on the surface and we consider the partition functions for translation and rotation in the adsorbed state to be unity. In that case the ratio $q^\ddagger/q_{\text{ads}}$ is maximized and calculation of the prefactor is simply a matter of calculating the 3D rotational and two-dimensional (2D) translational partition functions in the transition state (gas phase).

Using the partition functions in Eqs. (5) and (7) we thus calculate an upper limit on the prefactor, which we will call ν_{max} . Values for ν_{max} are listed in Table IV and plotted as a dashed line in Fig. 11. Compared to the prefactor values obtained from experiment as described above, we see that the

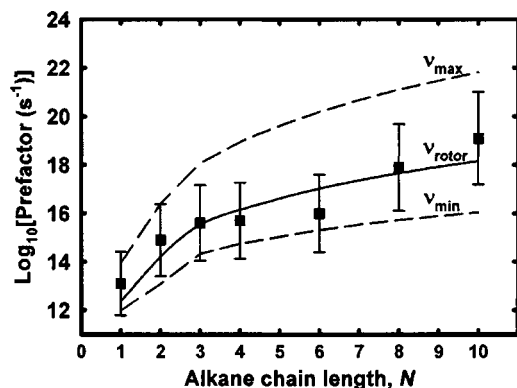


FIG. 11. Desorption prefactor vs alkane chain length. Experiment results are shown as solid squares with error bars. Upper and lower limits on the prefactor, ν_{max} and ν_{min} , are plotted as dashed lines. These are calculated by assuming that the sum of the rotational plus translational entropy of the molecule in the adsorbed state is a minimum or maximum, respectively. The solid curve, ν_{rotor} is based on a model where the adsorbed molecule has no rotational entropy on the surface but behaves translationally as a 2D gas. It is drawn to illustrate that the increase in prefactor with chain length can be accounted for entirely by considering the increase in rotational entropy available to the molecules in the 2D-gas transition state for desorption.

values for ν_{max} are uniformly larger by one to three orders of magnitude and that they have a stronger chain length dependence. We also note that for most of the alkanes studied, the values obtained for ν_{max} lie outside of the error bars of the prefactors determined experimentally. We conclude that this immobile adsorbate model overestimates the chain length dependence of the prefactor, but does provide its upper limit.

The opposite limit, ν_{min} is evaluated by considering the surface potential to have no corrugation parallel to the surface plane, but to bind the adsorbate strongly along the z axis (surface normal). In this case, the molecules will have the same translational degrees of freedom in the two dimensions parallel to the surface as they do in the gas phase. The contributions from the translational partition function to q^\ddagger and q_{ads} will cancel in the calculation of the prefactor [Eq. (3)]. On this corrugation-free surface, rotation about the z axis (helicopter mode) will also be freely accessible to the molecules and that dimension of rotational contribution to the prefactor will also cancel with the corresponding gas-phase partition function contribution. We have noted above that rotations about the x and y axes (log roll and cartwheel modes) will be more difficult for the longer alkanes ($N \geq 3$) as they each require that a significant fraction of the methyl and/or methylene groups moves away from the surface. Thus, for $N \geq 3$ we consider these rotations to be excluded and their contributions to the rotational partition functions to be one. Then the calculation of ν_{min} requires evaluation of the partition function for two rotational degrees of freedom in the gas phase. We consider ethane ($N=2$) to freely rotate about its C–C bond (x axis) on this corrugation-free model surface so that rotational contribution to q_{ads} has been included in the calculation of ν_{min} for $N=2$ and cancels with the corresponding contribution to q^\ddagger . Since methane (CH_4) is a spherical molecule we consider it to have free rotations about all three axes as well as 2D translations on the smooth surface. Then ν_{min} for methane is reduced to calculating $k_B T/h$ at the desorption temperature.

These results for ν_{min} are listed in Table IV and are plotted as a dashed line in Fig. 11. These values have a noticeable chain length dependence but not as strong as the experimental values. They fall within the error bars of four of the seven molecules studied, but are uniformly smaller than the experimentally obtained values.

It is clear that the MgO surface will have some surface corrugation, and therefore it is not surprising that the experimentally obtained prefactors exceed ν_{min} . Furthermore, from the TPD experiments at increasing initial coverage, it is clear that the adsorption sites with the highest binding energy (i.e., defects) are populated first. This indicates that the molecules have sufficient mobility on the surface to sample many sites, therefore the values of ν_{max} , obtained from the immobile adsorbate model, overestimate the prefactors. Thus, what is needed is a model wherein the initial adsorbed state has entropy intermediate between an immobile adsorbate and a 2D gas freely rotating about the z axis. We have noted previously that the increase in the translational partition function (or increase in translation entropy) with chain length cannot account for the strong rise in prefactor that we observe experimentally. Next, we construct a simple model to illustrate that the increase with chain length in the *rotational* entropy of the transition state alone can account for the prefactor increase.

For the purposes of this calculation, we make the assumption that the molecules have free translation on the surface, i.e., they behave translationally like a 2D gas, but that all rotation is prohibited. This assumption allows cancellation in Eq. (3) of the contributions to the partition functions from the two translational degrees of freedom parallel to the surface. Hence, calculation of $q^\ddagger/q_{\text{ads}}$ in Eq. (3) is reduced to calculating the rotational partition function of the molecule in the transition state (3D rotor in the gas phase). Prefactors evaluated in this manner at the desorption temperature of each molecule are listed as ν_{rotor} in Table IV and plotted as a function of alkane chain length in Fig. 11 (solid line). The prefactors calculated from this scenario exhibit excellent agreement with the results of the experimental analysis. This ν_{rotor} model is not intended to provide an accurate physical picture of the desorption mechanism, but rather to illustrate that the large increase in prefactor with chain length can be accounted for entirely by considering the increase in rotational entropy available to the molecules in the gas-phase-like transition state. It is hard to imagine a real adsorbate/substrate system where the interaction potential allows completely free translation of the adsorbate but no rotation at the same temperature. The real situation here probably corresponds instead to an interaction potential where both the translation and rotational modes are hindered to some degree in the adsorbed state at the desorption temperature. More detailed calculations would be required to determine the extent of translational and rotational freedom in the adsorbed state.

As we have noted, a rigorous theoretical investigation is needed to confidently calculate the partition functions and thereby obtain correct prefactors for the desorption of these molecules. We have presented upper and lower limits on the prefactors using simplified statistical mechanical models.

The actual values for the partition functions fall somewhere between these extrema. In any case, we have illustrated that the chain length dependence of the prefactor is significant and can be accounted for by considering the increase in the rotational entropy of the alkanes with chain length.

CONCLUSIONS

We have studied the desorption kinetics of *n*-alkanes (C_NH_{2N+2} , $N=1-4, 6, 8,$ and 10) from the MgO(100) surface. We find that the desorption temperature of the molecules increases with chain length. We have demonstrated the use of an optimization-inversion method for analysis of these TPD data which allows accurate determination of coverage-dependent desorption-kinetics parameters. Using these analysis results, we have demonstrated that we are able to accurately simulate the TPD experiments over a wide range of initial coverages and heating rates. We observe a linear increase in the desorption activation energy with alkane chain length, as has been noted in previous works on other surfaces, but unlike other works we see a small y -intercept value for $E_d(N)$ compared to previous values which have been unphysically large. This improvement is at least partially attributable to our allowing the prefactor to vary with chain length, rather than assuming a value of 10^{13} s^{-1} . By doing so we observe a strong increase in the desorption prefactor with chain length. We have also demonstrated that this increase can easily be accounted for by the large increase with chain length in the rotational entropy of the molecules in the gas-phase-like transition state.

ACKNOWLEDGMENTS

Two of the authors (B.D.K.) and (Z.D.) funded by the U.S. Department of Energy Office of Basic Energy Sciences (OBES) Chemical Sciences and Materials Sciences Divisions. One of the authors (C.T.C.) acknowledges support by the OBES Chemical Sciences Division. Another author (S.L.T.) supported by a graduate student fellowship award from the University of Washington/Pacific Northwest National Laboratory (PNNL) Joint Institute for Nanoscience and acknowledges participation in PNNL's Interfacial and Condensed Phase Chemical Physics Summer Research Insti-

tute. All of the experimental work was performed in the Environmental Molecular Sciences Laboratory, a national scientific user facility sponsored by the Department of Energy's Office of Biological and Environmental Research and located at PNNL. PNNL is a multiprogram National Laboratory operated for the U.S. Department of Energy by Battelle Memorial Institute under Contract No. DE-AC06-76RLO 1830.

- ¹A. R. Bishop, G. S. Girolami, and R. G. Nuzzo, *J. Phys. Chem. B* **104**, 754 (2000).
- ²J. F. Weaver, A. F. Carlsson, and R. J. Madix, *Surf. Sci. Rep.* **50**, 107 (2003).
- ³J. L. Brand, M. V. Arena, A. A. Deckert, and S. M. George, *J. Chem. Phys.* **92**, 5136 (1990).
- ⁴A. V. Teplyakov, A. B. Gurevich, M. X. Yang, B. E. Bent, and J. G. G. Chen, *Surf. Sci.* **396**, 340 (1998).
- ⁵B. A. Sexton and A. E. Hughes, *Surf. Sci.* **140**, 227 (1984).
- ⁶S. M. Wetterer, D. J. Lavrich, T. Cummings, S. L. Bernasek, and G. Scoles, *J. Phys. Chem. B* **102**, 9266 (1998).
- ⁷R. M. Slayton, C. M. Aubuchon, T. L. Camis, A. R. Noble, and N. J. Tro, *J. Phys. Chem.* **99**, 2151 (1995).
- ⁸K. R. Paserba and A. J. Gellman, *J. Chem. Phys.* **115**, 6737 (2001).
- ⁹K. R. Paserba and A. J. Gellman, *Phys. Rev. Lett.* **86**, 4338 (2001).
- ¹⁰*CRC Handbook of Chemistry and Physics* (CRC, Boca Raton, FL, 1972).
- ¹¹R. Z. Lei, A. J. Gellman, and B. E. Koel, *Surf. Sci.* **554**, 125 (2004).
- ¹²K. A. Fichthorn and R. A. Miron, *Phys. Rev. Lett.* **89**, 196103 (2002).
- ¹³S. L. Tait, Z. Dohnálek, C. T. Campbell, and B. D. Kay, *J. Chem. Phys.* **122**, 164707 (2005), preceding paper.
- ¹⁴Z. Dohnálek, G. A. Kimmel, S. A. Joyce, P. Ayotte, R. S. Smith, and B. D. Kay, *J. Phys. Chem. B* **105**, 3747 (2001).
- ¹⁵P. A. Redhead, *Vacuum* **12**, 203 (1962).
- ¹⁶D. A. King, *Surf. Sci.* **47**, 384 (1975).
- ¹⁷J. L. Falconer and R. J. Madix, *Surf. Sci.* **48**, 393 (1975).
- ¹⁸A. M. de Jong and J. W. Niemantsverdriet, *Surf. Sci.* **233**, 355 (1990).
- ¹⁹J. L. Taylor and W. H. Weinberg, *Surf. Sci.* **78**, 259 (1978).
- ²⁰R. N. Carter and A. B. Anton, *J. Vac. Sci. Technol. A* **10**, 344 (1992).
- ²¹D. A. McQuarrie, *Statistical Mechanics* (Harper & Row, New York, 1975).
- ²²C. T. Campbell, Y.-K. Sun, and W. H. Weinberg, *Chem. Phys. Lett.* **179**, 53 (1991).
- ²³R. I. Masel, *Principles of Adsorption and Reaction on Solid Surfaces* (Wiley, New York, 1996).
- ²⁴P. W. Atkins, *Physical Chemistry* (Oxford University Press, Oxford, 1978).
- ²⁵J. B. Hendrickson, D. J. Cram, and G. S. Hammond, *Organic Chemistry* (McGraw-Hill, New York, 1970).
- ²⁶P. J. Flory, *Statistical Mechanics of Chain Molecules* (Hanser Publishers, Munich, 1988).
- ²⁷J. S. Raut and K. A. Fichthorn, *J. Chem. Phys.* **108**, 1626 (1998).